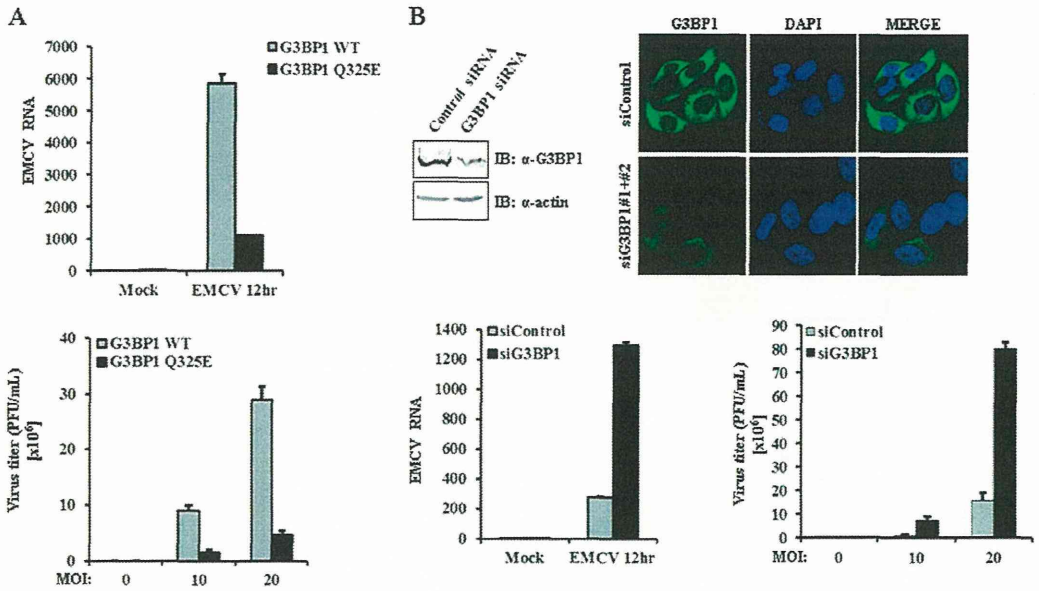

FIG 5 Cleavage or knockdown of G3BP1 results in enhanced EMCV replication. (A) HeLa/G-G3BP1 and HeLa/G-G3BP1Q325E cells were infected with EMCV. (Top) Total RNA was harvested at 12 h postinfection, and EMCV RNA was quantified by qPCR. (Bottom) The culture supernatant was subjected to plaque titration. (B) HeLa cells were transfected with either control siRNA or siRNA that targeted G3BP1. (Top) After 48 h, G3BP1 was detected by Western blotting (left) or by staining using anti-G3BP1 antibody (right). (Bottom, left) To investigate the effect of G3BP1 knockdown on viral replication, the cells were infected with EMCV for 12 h, total RNA was extracted, and EMCV RNA was quantified by qPCR. (Right) The culture supernatant was analyzed to determine viral titers.

Tris-HCl [pH 9.0], 150 mM NaCl, 1 mM $MgCl_2$, 66 μl of NBT [50 mg/ml], and 33 μl of BCIP [50 mg/ml]).

Antibodies. The antibodies used in this study include mouse monoclonal anti-green fluorescent protein (GFP) (1:1,000 dilution) (MBL), goat polyclonal anti-G3BP1 (1:500) (catalog no. sc-70283; Santa Cruz), mouse monoclonal anti-G3BP1 (1:1,000) (catalog no. sc-365338; Santa Cruz), rabbit polyclonal anti-PKR (1:1,000) (catalog no. sc-709; Santa Cruz), rabbit polyclonal anti-TIA-1/R (1:1,000) (catalog no. sc-48371; Santa Cruz), goat polyclonal anti-TIAR (1:1,000) (catalog no. sc-1749; Santa Cruz), rabbit polyclonal anti-HuR (1:1,000) (catalog no. sc-365816; Santa Cruz), and propidium iodide (PI) (1:2,000 in PBST) (Miltenyi Biotec). The RIG-I antibodies were generated by immunizing a rabbit with a synthetic peptide corresponding to amino acids 793 to 807 of RIG-I and MDA5. Mouse monoclonal anti-poly(A) binding protein (PABP) (1:1,000) (catalog number ab6125; Abcam), rabbit monoclonal antiactin (1:5,000) (Poly6221; BioLegend), mouse anti-FLAG (1:1,000) (Sigma-Aldrich), and rabbit monoclonal anti-phospho-PKR pT446 (1:1,000) (Epitomics Inc.) antibodies were also used. Anti-EMCV polyclonal antibody was obtained by immunizing a rabbit with purified EMCV virions. Anti-MDA5 polyclonal antibody was obtained by immunizing a rat with recombinant MDA5 (produced in insect cells), which was preactivated with RNA ligands.

Quantification of the distribution pattern of virus-induced SGs. SG formation was quantified visually by using eyesight counting. The total number of cells displaying each unique distribution pattern in each location was recorded, and the percentage of each pattern was calculated. As for the fixed cells, 10 pictures were taken randomly at different locations. Cells displaying SG foci were quantified manually. Graphs display the average percentages of replicates (at least 20 times).

RESULTS

Characterization of HeLa cells stably expressing an SG marker, G3BP1. To monitor SGs in living cells, we generated HeLa/G-G3BP cells (Fig. 1). Constitutive aggregation of intrinsic SG components has been reported to lead to a severe stall in protein synthesis and eventual apoptosis (14, 20). All the HeLa/G-G3BP clones displayed uniform and high-level GFP expression, and their growth rate was comparable to that of parental cells (our unpublished observations). It has been well documented that G3BP1 accumulates in SG foci in response to arsenite treatment (oxidative stress) and virus infection (12, 13). HeLa/G-G3BP clone 12 was treated with arsenite or infected with Newcastle disease virus (NDV) or influenza A virus (IAV) with an NS1 deletion (IAVΔNS1), and GFP localization was then examined by confocal microscopy. As shown in Fig. 1A, a speckle-like localization of GFP was induced by these stimuli. Other clones also exhibited similar speckle formation after arsenite treatment or NDV infection (Fig. 1B and C). We confirmed that other SG components, TIA-1, TIAR, HuR, and eIF3, colocalized with the GFP speckles (our unpublished observations). These results indicate that EGFP-G3BP1 acts as a suitable probe for virus-induced SGs. However, since transient overexpression of G3BP1 results in SG formation without external stress (13), we tested if the HeLa/G-G3BP clones would exhibit a normal antiviral response. As shown in Fig. 1D, all clones exhibited induction of IFN-β mRNA comparable to that exhibited by parental cells. We chose clone 18 for further analyses.

G3BP1 exhibits three redistribution patterns after infection with both RNA and DNA viruses. To examine the dynamics of cytoplasmic SGs induced by viral infection, the cells were infected with different viruses, as shown in Fig. 2, and monitored live for distribution of GFP fluorescence (representative results are shown in Movies S1 to S9 in the supplemental material). Cells infected with SeV, IAV, VSV, and TMEV did not show SG formation (8). Other viruses induced SGs, typically forming a large number of small granules at around 5 h postinfection and gradually fusing to each other. SG formation was quantified (Fig. 2A to K) and clas-

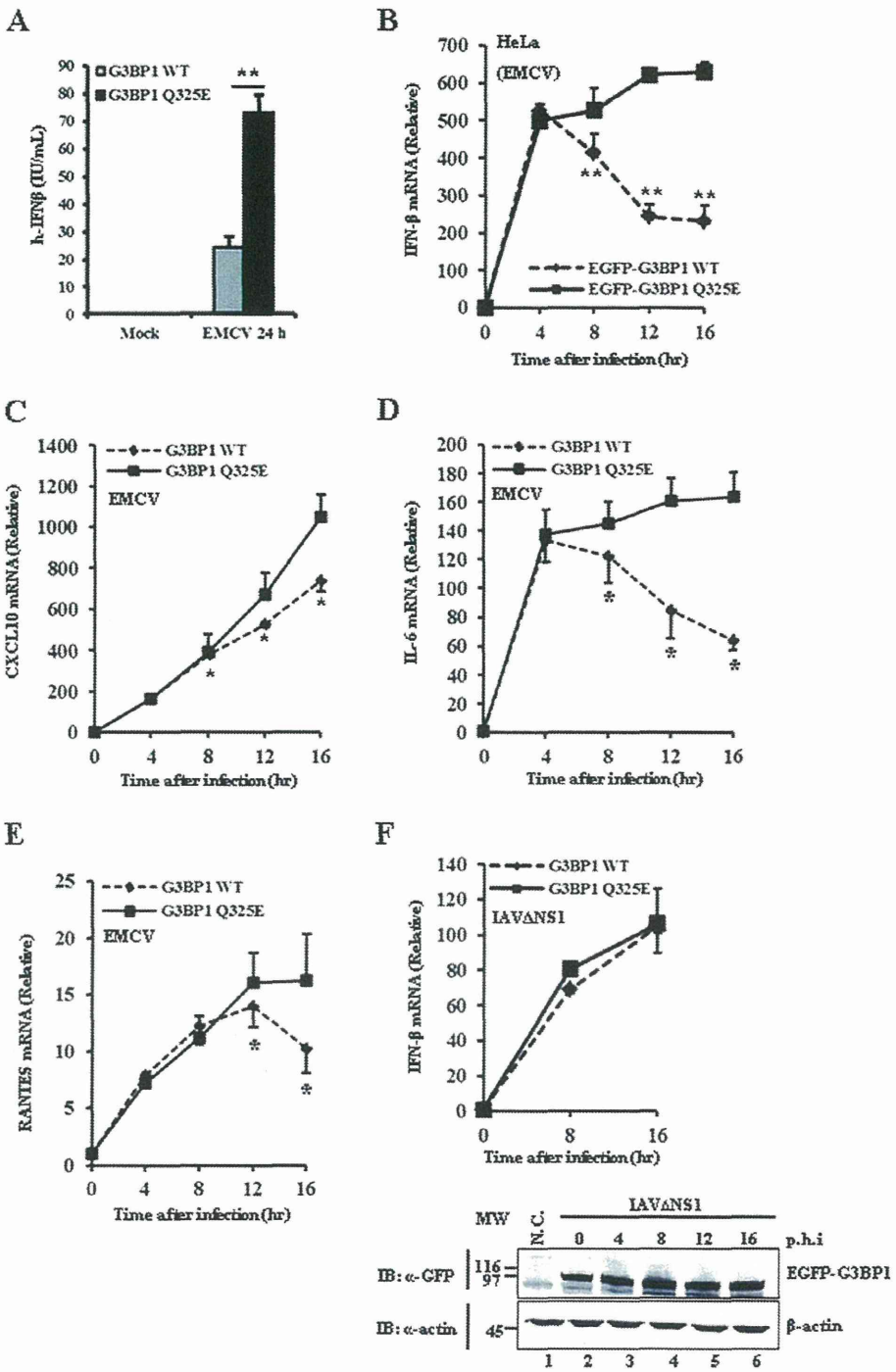

FIG 6 Inhibition of G3BP1 in EMCV-infected cells results in sustained cytokine/chemokine mRNA accumulation. HeLa/G-G3BP1 and HeLa/G-G3BP1Q325E cells were infected with EMCV. (A) Culture supernatant was subjected to an enzyme-linked immunosorbent assay for human IFN-β (hIFN-β). (B to E) Total RNA was harvested at the indicated time points. mRNA levels for IFN-β (B), CXCL10 (C), IL-6 (D), and RANTES (E) were determined by RT-qPCR. (F, left) Both HeLa/G-G3BP and HeLa/G-G3BPQ325E cells were infected with IAVΔNS1, and the IFN-β mRNA level was quantified as described above. (Right) Lysates of IAVΔNS1-infected HeLa/G-G3BP1 cells were examined for cleavage of G3BP1 by Western blotting. Data depicted are representative of two independent experiments. (Error bars indicate standard deviations of duplicates.) **, $P < 0.005$; *, $P < 0.05$.

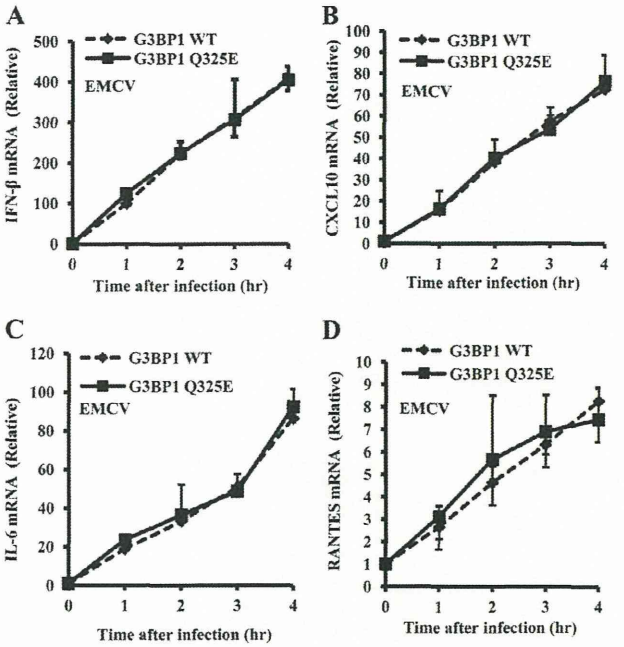

FIG 7 IFN production and cytokine gene activation in HeLa/G-G3BP and HeLa/G-G3BPQ325E cells at the early phase. HeLa/G-G3BP1 and HeLa/G-G3BP1Q325E cells were mock treated or infected with EMCV for the indicated times. Total RNA was extracted, and mRNA levels for IFN-β (A), CXCL10 (B), IL-6 (C), and RANTES (D) were quantified by RT-qPCR.

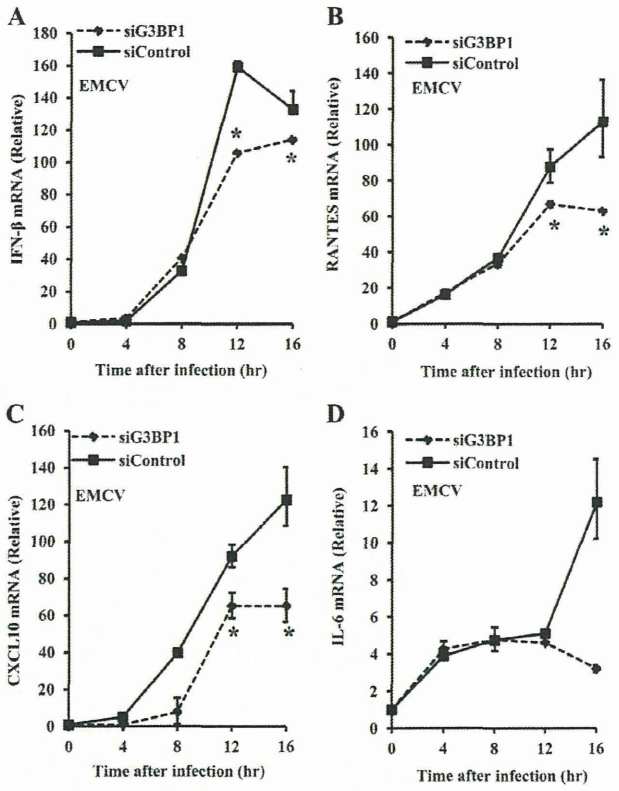

FIG 8 Knockdown of G3BP1 attenuates EMCV-induced cytokine/chemokine gene activation. HeLa cells were transfected with either control siRNA or siRNA that targeted G3BP1. After 48 h of incubation, cells were infected with EMCV for 12 h, and total RNA was collected as indicated. mRNAs levels for IFN-β (A), RANTES (B), CXCL10 (C), and IL-6 (D) were determined by RT-qPCR. Data are representative of two independent experiments. (Error bars indicate standard deviations of duplicates [$n = 2$].) *, $P < 0.05$.

sified into three predominant patterns, stable formation (Fig. 2L), transient formation (Fig. 2M), and alternating formation (Fig. 2N), within a single cell. NDV, IAVΔNS1, and adenovirus type 5 displayed stable formation of SGs (see Movies S1 to S3 in the supplemental material). Whereas SINV, EMCV, and PolioV induced foci at around 5 to 6 h postinfection, the foci disappeared thereafter (transient formation) (Fig. 2D to F; see also Movies S4 to S6 in the supplemental material). Interestingly, adenovirus type 5 with an E1A deletion exhibited multiple rounds of formation and disappearance of SGs (alternate formation) in the majority of cells (Fig. 2I; see also Movie S7 in the supplemental material). A similar oscillation of SGs in cells infected with hepatitis C virus (HCV) and treated with IFN was reported previously (21). Collectively, these live-cell-imaging analyses demonstrated that viral infections trigger host stress responses; however, different viruses induce distinct response patterns, presumably through specific underlying mechanisms. The observed SG formation patterns are unlikely to be due to G3BP1 overexpression, because wt HeLa cells exhibited transient SG formation upon EMCV infection when endogenous G3BP1 was used as a marker (Fig. 2O).

EMCV infection results in the cleavage of G3BP1. We focused on the mechanism of transient formation of SGs by EMCV because PolioV has been reported to inhibit SG formation by cleavage of G3BP1 (15). We examined if EGFP-G3BP1 is cleaved by EMCV by Western blotting. The EGFP-G3BP1 fusion protein is detected as a polypeptide of 96 kDa, and EMCV infection resulted in the appearance of an 80-kDa GFP-containing protein at 6 h postinfection, and nearly complete cleavage of EGFP-G3BP1 occurred at 10 h postinfection (Fig. 3A). Because the fusion protein contains an EGFP moiety at the N terminus of G3BP, the cleavage of G3BP1 is likely to occur at the C-terminal region of G3BP1. We verified the cleavage site by using an antibody detecting the C-terminal epitope of G3BP1 (see Fig. S1A and S1B in the supplemental material). Because the mapped cleavage site was close to that of PolioV and cleavage by PolioV is prevented by an amino acid substitution within G3BP1 (Q325E) (15), we therefore examined this mutant for cleavage by EMCV (Fig. 3B). We found that the G3BP1 Q325E mutant was resistant to cleavage by EMCV, suggesting a common cleavage mechanism. To examine whether the disruption of SGs by EMCV is due solely to cleavage of G3BP1, we examined other SG components, such as PABP, TIA-1/R, HuR, and PKR, which are also essential for SG formation. Figure 3C shows that the levels of SG components, with the exception of G3BP1, did not change upon EMCV infection and that G3BP1 cleavage coincided with the detection of EMCV proteins. Expression of EMCV 3C protease but not leader protein by transfection was sufficient to reproduce G3BP1 cleavage at Q325 (Fig. 3D), strongly suggesting that the cleavage is mediated by 3C protease. We next examined SG formation of HeLa/G-G3BPQ325E cells. In sharp contrast to cells expressing wild-type G3BP1 (see Movie S6 in the supplemental material), HeLa/G-G3BPQ325E cells exhibited stable formation of SGs, as judged by single-cell imaging (Fig. 4A and B; see also Movie S8 in the supplemental material) and

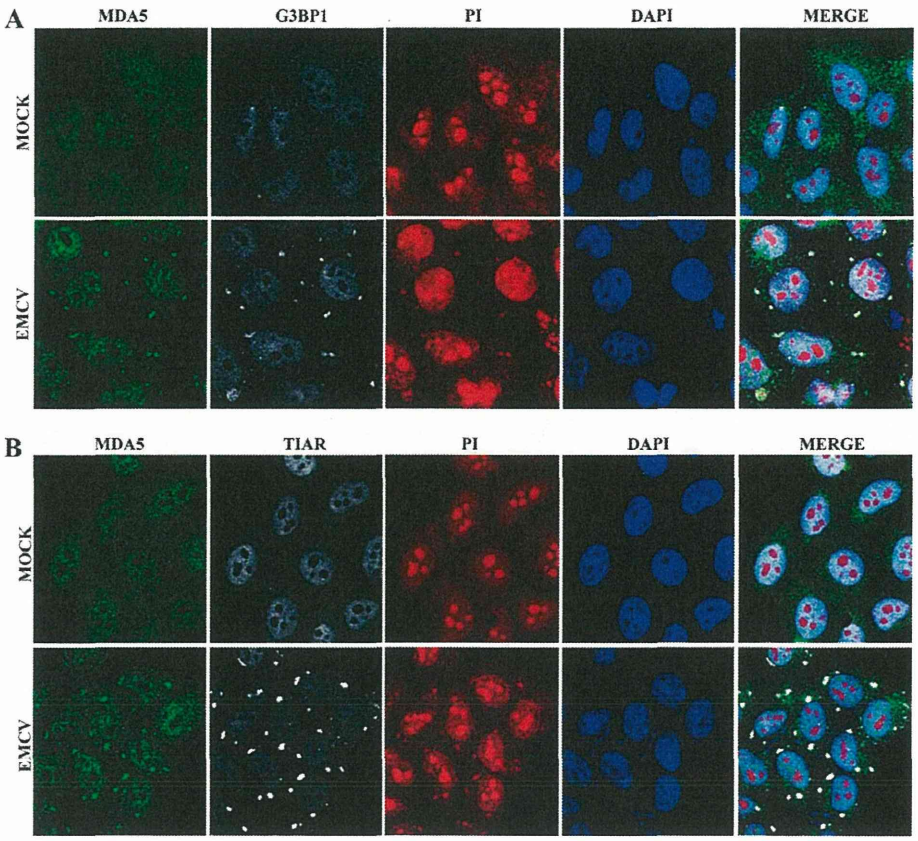

FIG 9 EMCV infection recruits MDA5 into SGs. HeLa cells were mock treated or infected with EMCV (MOI of 10) and fixed. The cells were stained for MDA5, G3BP1, and PI (A) or MDA5, TIAR, and PI (B).

quantification (Fig. 4C). These results suggest that EMCV disrupts SGs by cleavage of G3BP1 through a mechanism similar to that of PolioV.

G3BP1 negatively regulates EMCV replication. To examine the impact of SG disruption on EMCV replication, we infected both HeLa/G-G3BP and HeLa/G-G3BPQ325E cells with EMCV and analyzed viral replication by RT-qPCR (Fig. 5A). The EMCV RNA level recovered from HeLa/G-G3BP cells was 6-fold higher than that recovered from HeLa/G-G3BPQ325E cells. Similarly, a significantly lower viral yield was observed for cells expressing G3BP1 Q325E, suggesting that SG formation is critical for suppressing EMCV replication. To further confirm the involvement of G3BP1, we depleted endogenous G3BP1 by siRNA-mediated knockdown (Fig. 5B) and examined its effect on EMCV replication. G3BP1 knockdown caused increased EMCV replication, as judged by the approximately 5-fold augmentation of viral RNA and viral yield (Fig. 5B). These results suggest that G3BP1 is involved in the negative regulation of EMCV.

G3BP1 is critical for EMCV-induced interferon and cytokine gene activation. Based on the above-described findings, we next asked how G3BP1 exerts its antiviral role. The type I interferon system constitutes major innate antiviral responses; therefore, we examined EMCV-induced IFN-β gene activation in HeLa/G-G3BP and HeLa/G-G3BPQ325E cells (Fig. 6). In HeLa/G-G3BP cells, IFN-β mRNA accumulated at 4 h postinfection, followed by a gradual decrease. However, IFN-β mRNA levels persisted in HeLa/G-G3BPQ325E cells after 8 h postinfection (Fig. 6B). In agreement with these results, the amount of IFN-β protein released into the culture medium at 24 h was significantly augmented by the Q325E mutation (Fig. 6A). A similar enhancement of cytokine mRNA was observed for CXCL10, interleukin-6 (IL-6), and RANTES (Fig. 6C to E). We investigated gene activation at early time points between 0 and 4 h and observed similar activation kinetics between HeLa/G-G3BP and HeLa/G-G3BPQ325E cells (Fig. 7), suggesting that the reduced gene activation of HeLa/G-G3BP cells is due to G3BP1 cleavage. The Q325E mutation did not affect IFN-β gene induction in the case of IAVΔNS1, which did not cause G3BP1 cleavage (Fig. 6F). Next, we examined the effects of depletion of endogenous G3BP1 on cytokine gene activation. As expected, knockdown of endogenous G3BP1 attenuated the expression of IFN-β and other cytokine genes (Fig. 8A to D). These results strongly suggest that G3BP cleavage leads to attenuation of antiviral cytokine induction.

It has been well documented that MDA5 senses EMCV infection (22–25) and that virus- and oxidative stress-induced SGs recruit RIG-I, MDA5, and LGP2 (12). Therefore, we hypothesized that EMCV-induced SG regulates IFN-β gene activation by facilitating MDA5 activation. We examined MDA5 localization in EMCV-infected HeLa cells by immunostaining. MDA5 displayed relocalization to speckle-like granules upon EMCV infection (Fig. 9A). The speckles also contained endogenous G3BP1 (Fig. 9A) and TIAR (Fig. 9B). Interestingly, PI, a

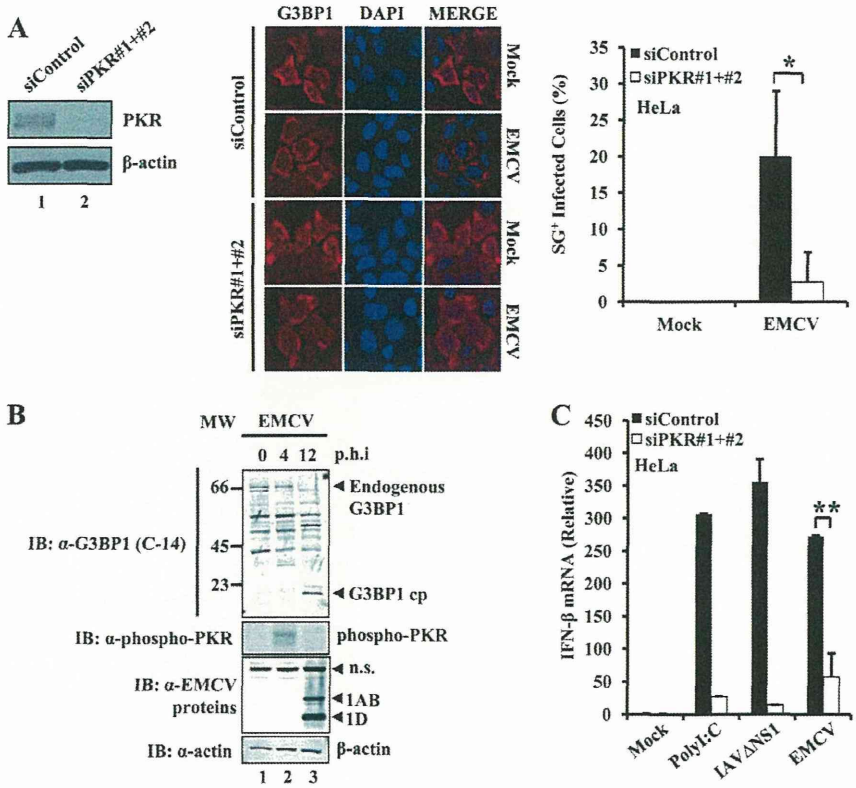

FIG 10 Involvement of PKR in EMCV-induced SG and IFN-β gene activation. (A) Knockdown of PKR expression results in reduced SGs. (Left) HeLa cells transfected with siRNA targeting PKR for 48 h were examined for PKR expression by Western blotting. (Middle) The cells were infected with EMCV for 6 h and stained for endogenous G3BP1. (Right) SG-containing cells were quantified. (B) HeLa cells infected with EMCV for 0, 4, and 12 h were analyzed for G3BP1, phospho-PKR, EMCV proteins, and actin by immunoblotting. (C) HeLa cells transfected with siRNA targeting PKR for 48 h were mock treated, transfected with poly(I·C), or infected with IAVΔNS1 or EMCV. After 12 h, IFN mRNA was quantified by RT-qPCR. **, $P < 0.005$; *, $P < 0.05$.

dye that binds to dsDNA and dsRNA, stains cytoplasmic speckles found only in virus-infected cells, and the dsRNA speckles colocalized with G3BP1 and TIAR. These observations suggest that EMCV infection induces SGs, which recruit SG components, MDA5, and EMCV dsRNA.

PKR is essential for SG formation and IFN induction in EMCV infection. Various types of viruses were shown to induce SG formation through PKR activation (26–28). We therefore examined whether EMCV induces SG formation in a PKR-dependent manner. Endogenous PKR expression was efficiently downregulated by siRNA (Fig. 10A). Under these conditions, SG formation by EMCV was decreased significantly (Fig. 10A). We next asked whether cleavage of G3BP1 results in PKR dephosphorylation. Immunoblot analyses showed that PKR was autophosphorylated at 4 h postinfection; however, at 12 h, when G3BP1 cleavage was nearly complete, PKR phosphorylation was undetectable (Fig. 10B, lane 3), suggesting that G3BP1 cleavage resulted in PKR dephosphorylation. Finally, we examined whether the final outcome of signaling, IFN-β gene expression, was dependent on PKR. In PKR knockdown cells, the induction of IFN-β mRNA by EMCV was significantly decreased compared to that in control cells (Fig. 10C). We further confirmed previous reports that IFN induction by poly(I·C) or IAVΔNS1 infection was PKR dependent (12). From the data presented above, we concluded that the loss of PKR impaired EMCV-induced SG formation, leading to a reduction of IFN-β gene activation.

DISCUSSION

Viral infection causes stress in host cells, resulting in SG formation. To date, both pro- and antiviral roles have been described for virus-induced SGs (28–30), and this issue remains controversial.

In this study, we demonstrated that SGs are potentially involved in mediating virus-triggered IFN responses. It was reported previously that PolioV 3C protease cleaves G3BP1 at residue Q325, resulting in the disruption of SGs (15). This observation indicates not only that G3BP1 is a component of SGs but also that its inactivation by cleavage causes the disruption of SGs. Here, we show that EMCV shares G3BP cleavage activity with specificity identical to that of PolioV 3C, requiring intact Q325. Interestingly, coxsackievirus also disrupts SGs (31) by a similar mechanism (G. Fung, C. S. Ng, J. Zhang, J. Shi, J. Wong, P. Piesik, L. Han, F. Chu, J. Jagdeo, E. Jan, T. Fujita, and H. Luo, unpublished observation), suggesting that this strategy is shared by some picornaviruses to evade immune responses. At the early phase of EMCV infection, cleavage of G3BP1 was not evident. However, at 4 h postinfection, cleavage was detectable, and at 10 h, cleavage reached completion, suggesting that the accumulation of 3C is necessary for the disruption. We observed that stable expression of the G3BP1 Q325E mutant blocked the disassembly of SGs as well as enhanced IFN-β production at a late phase of infection. Furthermore,

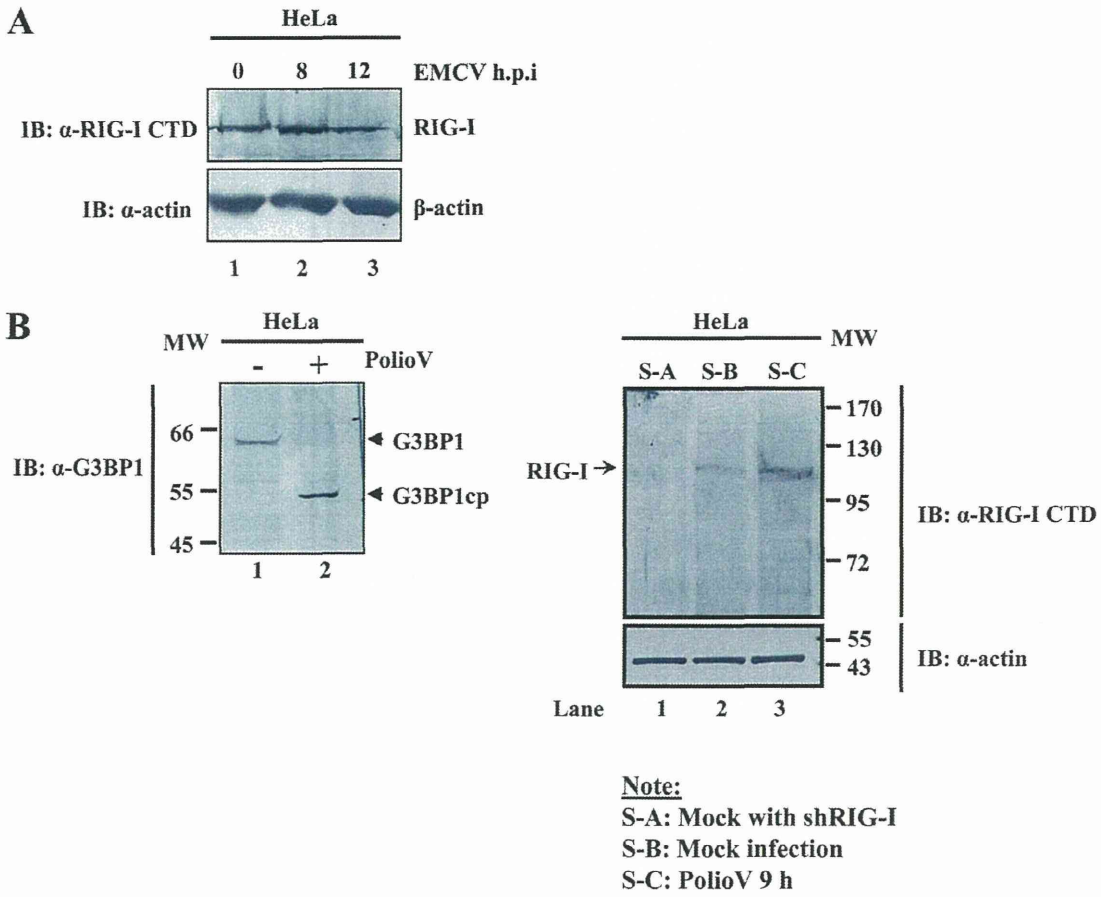

FIG 11 RIG-I was not cleaved after EMCV or PolioV infection. (A) HeLa cells were either mock treated or infected with EMCV for the indicated times. RIG-I was detected by Western blotting. (B) HeLa cells were mock treated or infected with PolioV for 9 h. G3BP1 (left) and RIG-I (right) were examined by Western blotting. CTD, C-terminal domain; shRIG-I, short-hairpin RIG-I.

knockdown experiments showed that G3BP1 is necessary for efficient activation of the IFN-β gene, particularly in the later stages of infection. Although it was reported previously that PolioV 3C cleaves RIG-I and MDA5 (32) and that EMCV cleaves RIG-I (33), we did not observe these cleavages, even under conditions in which G3BP1 was cleaved by EMCV or PolioV (Fig. 11). Taken together, we conclude that G3BP1 is a physiological regulator of IFN-β gene induction through the formation of SGs, which recruit the RNA sensor MDA5. In addition, the persistent activation of the IFN-β gene at late time points is likely due to the increase of the local concentrations of both MDA5 and its ligands within the condensed granules.

Collectively, the data presented above strongly suggest that 3C protease of EMCV acts as a critical factor for evading host IFN production to ensure efficient replication. It was demonstrated previously that PKR plays a critical role in dsRNA- or IAVΔNS1-induced SG formation and subsequent IFN-β gene activation (12). Our observation that PKR is required for efficient IFN gene activation by EMCV suggests that PKR is responsible for initiating SG formation (Fig. 10).

Considering that the assembly of SGs is a part of the antiviral response of the host, it is plausible that viruses evolve strategies to block it. Indeed, IAV, SeV, and TMEV do not induce SG (Fig. 2), and it was reported previously that leader RNA, NS1, and leader protein are responsible for inhibition, respectively (8, 12, 34). Although TMEV belongs to the *Picornaviridae*, its mechanism of SG inhibition appeared to be distinct from those of EMCV and PolioV. TMEV and mengovirus inhibit SG by the action of leader protein (8, 31). We found that 3C but not the leader protein of EMCV inhibits SG formation (Fig. 12). It is tempting to speculate that leader proteins of TMEV and mengovirus inhibit IFN production (35, 36) through the blockade of SG formation, where RLR and viral RNA efficiently interact, as one of the mechanisms. Interestingly, although the leader protein of EMCV did not affect SGs, it inhibited IFN gene activation (Fig. 12), suggesting that leaders of different cardioviruses are functionally equivalent (37, 38) but with distinct modes of action. Therefore, these viruses encode multiple inhibitory proteins to efficiently manipulate host immune responses. EMCV and SINV induced SGs at early time points after infection, but SG formation was disrupted later. A similar phenomenon was reported previously for West Nile and dengue viruses by monitoring TIA-1/R as an SG marker (29). In the case of EMCV and PolioV, G3BP1 cleavage by viral 3C protease is responsible for the disassembly of SGs. Therefore, active mechanisms for the disruption of SGs by SINV, West Nile virus, and dengue virus have been suggested, although the underlying mechanisms remain to be determined. In addition to transient

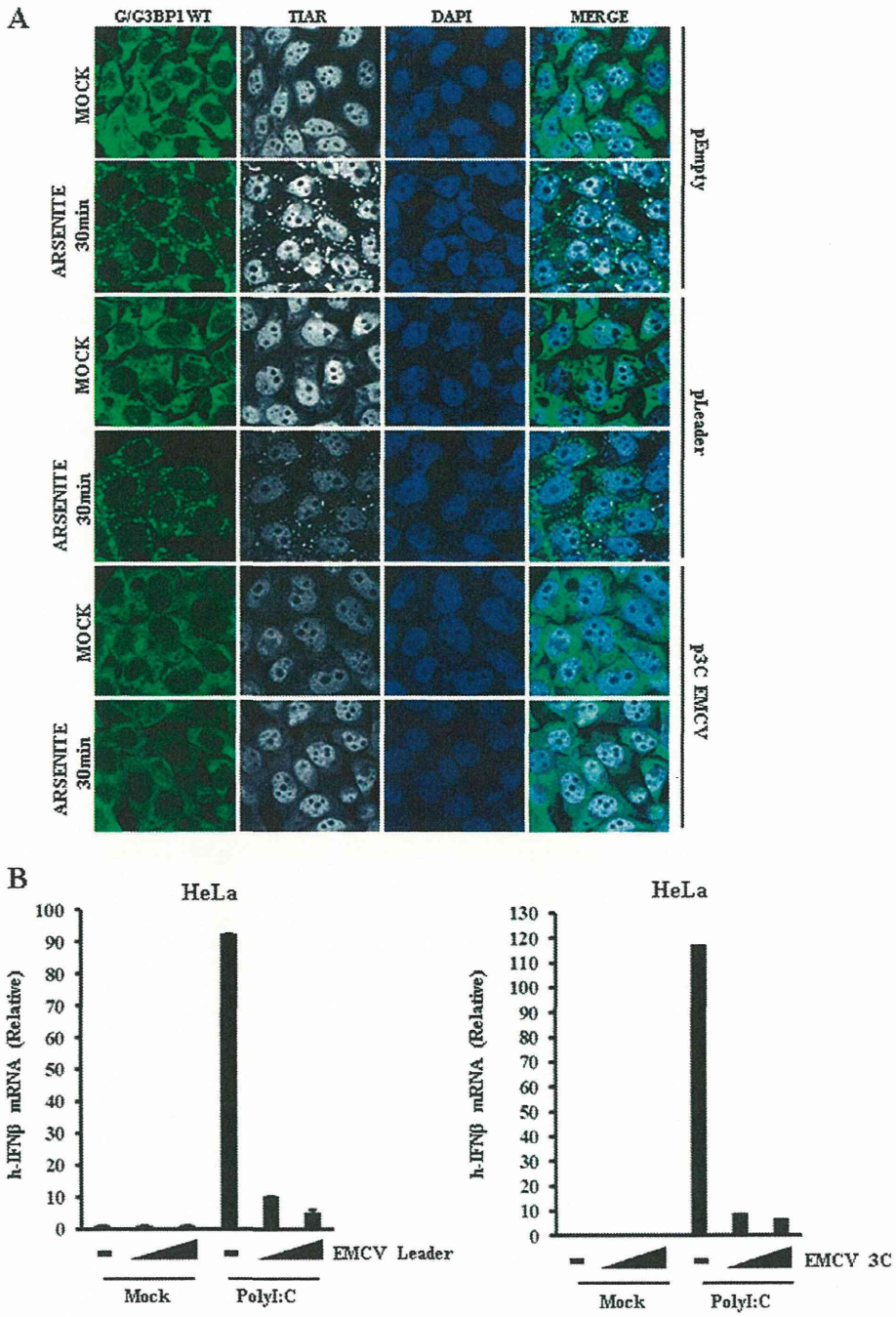

FIG 12 EMCV 3C but not leader inhibits SG. (A) HeLa/G-G3BP1 and HeLa/G-G3BP1Q325E cells were transiently transfected with an empty vector or the expression vector for leader or 3C for 48 h. Cells were treated with 0.5 mM sodium arsenite for 30 min, fixed, and stained for TIAR, an SG marker. (B) HeLa cells were transiently transfected with and empty vector or the expression vector for leader or 3C (0 μg, 2 μg, and 4 μg) for 48 h. Cells were mock treated or transfected with long poly(I·C) (2 μg/μl) for 12 h. Total RNA was collected, and the mRNA level for IFN-β was determined by RT-qPCR. Data are representative of three independent experiments. (Error bars indicate standard deviations of duplicates [$n = 3$].)

formation of SGs, some viruses exhibited alternating formations of SGs; SGs were formed at an early stage and then disappeared and re-formed at a later stage. This alternating pattern is also dependent on the cell lines used (our unpublished observations), suggesting that the pattern of SG formation is determined by a dynamic balance between the host antiviral response and the viral inhibitory mechanism (21). Such a host mechanism could be a therapeutic target to enhance host defense against viruses.

Here, we provide evidence that EMCV-induced SGs are involved in regulating IFN-β gene expression. Thus, virus-induced

SGs might play dual roles: (i) suppressing viral replication through an inhibition of viral protein synthesis and (ii) serving as a platform to facilitate IFN-β production.

ACKNOWLEDGMENTS

We thank Jamal Tazi for providing pEGFP-G3BP1, A. C. Palmenberg for expression vectors for EMCV leader and 3C proteins, and Gabriel Fung (University of British Columbia) and Peter Gee (Kyoto University) for proofreading the manuscript.

This research was supported by grants from the Ministry of Education, Culture, Sports, Science and Technology (MEXT) of Japan (innovative areas, infection competency [no. 24115004] and scientific research A [no. 23249023]); the Ministry of Health, Labor and Welfare of Japan; the Uehara Memorial Foundation; the Mochida Memorial Foundation for Medical and Pharmaceutical Research; the Takeda Science Foundation; the Naito Foundation; and Nippon Boehringer Ingelheim. C.S.N. is a recipient of a Monbukagakusho fellowship from the MEXT. We declare that we have no conflicts of interest.

REFERENCES

1. Meylan E, Tschopp J, Karin M. 2006. Intracellular pattern recognition receptors in the host response. Nature 442:39–44.
2. Darnell JE, Jr, Kerr IM, Stark GR. 1994. Jak-STAT pathways and transcriptional activation in response to IFNs and other extracellular signaling proteins. Science 264:1415–1421.
3. Garcia MA, Gil J, Ventoso GI, Guerra S, Domingo E, Rivas C, Esteban M. 2006. Impact of protein kinase PKR in cell biology: from antiviral to antiproliferative action. Microbiol. Mol. Biol. Rev. 70:1032–1060.
4. Der S, Lau AS. 1995. Involvement of the double-stranded-RNA-dependent kinase PKR in interferon expression and interferon-mediated antiviral activity. Proc. Natl. Acad. Sci. U. S. A. 92:8841–8845.
5. Terenzi F, DeVeer M, Ying H, Restifo NP, Williams BR, Silverman RH. 1999. The antiviral enzymes PKR and RNase L suppress gene expression from viral and non-viral based vectors. Nucleic Acids Res. 27:4369–4375.
6. McInerney GM, Kedersha NL, Kaufman RJ, Anderson P, Liljeström P. 2005. Importance of eIF2α phosphorylation and stress granule assembly in alphavirus translation regulation. Mol. Biol. Cell 16:3753–3763.
7. White JP, Lloyd RE. 2012. Regulation of stress granules in virus systems. Trends Microbiol. 20:175–183.
8. Borghese F, Michiels T. 2011. The leader protein of cardioviruses inhibits stress granule assembly. J. Virol. 85:9614–9622.
9. Katoh H, Okamoto T, Fukuhara T, Kamban H, Morita E, Mori Y, Kamitani W, Matsuura Y. 2013. Japanese encephalitis virus core protein inhibits stress granule formation through an interaction with Caprin-1 and facilitates viral propagation. J. Virol. 87:489–502.
10. Okonski KM, Samuel CE. 2013. Stress granule formation induced by measles virus is protein kinase PKR dependent and impaired by RNA adenosine deaminase ADAR1. J. Virol. 87:756–766.
11. Dinh PX, Beura LK, Das PB, Panda D, Das A, Pattnaik AK. 2013. Induction of stress granule-like structures in vesicular stomatitis virus-infected cells. J. Virol. 87:372–383.
12. Onomoto K, Jogi M, Yoo JS, Narita R, Morimoto S, Takemura A, Sambhara S, Kawaguchi A, Osari S, Nagata K, Matsumiya T, Namiki H, Yoneyama M, Fujita T. 2012. Critical role of an antiviral stress granule containing RIG-I and PKR in viral detection and innate immunity. PLoS One 7:e43031. doi:10.1371/journal.pone.0043031.
13. Tourrière H, Chebli K, Zekri L, Courselaud B, Blanchard JM, Bertrand E, Tazi J. 2003. The RasGAP-associated endoribonuclease G3BP assembles stress granules. J. Cell Biol. 160:823–831.
14. Kedersha N, Tisdale S, Hickman T, Anderson P. 2008. Real-time and quantitative imaging of mammalian stress granules and processing bodies. Methods Enzymol. 448:521–552.
15. White JP, Cardenas AM, Marissen WE, Lloyd RE. 2007. Inhibition of cytoplasmic mRNA stress granule formation by a viral proteinase. Cell Host Microbe 15:295–305.
16. Porter FW, Bochkov YA, Albee AJ, Wiese C, Palmenberg AC. 2006. A picornavirus protein interacts with Ran-GTPase and disrupts nucleocytoplasmic transport. Proc. Natl. Acad. Sci. U. S. A. 103:12417–12422.
17. Ouda R, Onomoto K, Takahasi K, Edwards MR, Kato H, Yoneyama M, Fujita T. 2011. Retinoic acid-inducible gene I-inducible miR-23b inhibits infections by minor group rhinoviruses through down-regulation of the very low density lipoprotein receptor. J. Biol. Chem. 286:26210–26219.
18. Garcia-Sastre A, Egorov A, Matassov D, Brandt S, Levy DE, Durbin JE, Palese P, Muster T. 1998. Influenza A virus lacking the NS1 gene replicates in interferon-deficient systems. Virology 252:324–330.
19. Tisoncik JR, Billharz R, Burmakina S, Belisie SE, Proll SC, Korth MJ, Garcia-Sastre A, Katze MG. 2011. The NS1 protein influenza A virus suppresses interferon-regulated activation of antigen-presentation and immune-proteasome pathways. J. Gen. Virol. 92:2093–2104.
20. Kharraz Y, Salmand PA, Camus A, Auriol J, Gueydan C, Kruys V, Morello D. 2010. Impaired embryonic development in mice overexpressing the RNA-binding TIAR. PLoS One 5:e11352. doi:10.1371/journal.pone.0011352.
21. Ruggieri A, Dazert E, Metz P, Hofmann S, Bergeest JP, Mazur J, Bankhead P, Hiet MS, Kallis S, Alvisi G, Samuel CE, Lohmann V, Kaderali L, Rohr K, Frese M, Stoecklin G, Bartenschlager R. 2012. Dynamic oscillation of translation and stress granule formation mark the cellular response to virus infection. Cell Host Microbe 12:71–85.
22. Kato H, Sato S, Yoneyama M, Yamamoto M, Uematsu S, Matsui K, Tsujimura T, Takeda K, Fujita T, Takeuchi O, Akira S. 2005. Cell type-specific involvement of RIG-I in antiviral response. Immunity 23:19–28.
23. Kato H, Takeuchi O, Sato S, Yoneyama M, Yamamoto M, Matsui K, Uematsu S, Jung A, Kawai T, Ishii KJ, Yamaguchi O, Otsu K, Tsujimura T, Koh CS, Reis e Sousa C, Matsuura Y, Fujita T, Akira S. 2006. Differential roles of MDA5 and RIG-I helicases in the recognition of RNA viruses. Nature 441:101–105.
24. Ng CS, Kato H, Fujita T. 2012. Recognition of viruses in the cytoplasm by RLRs and other helicases—how conformational changes, mitochondrial dynamics and ubiquitination control innate immune responses. Int. Immunol. 24:739–749.
25. Feng Q, Hato SV, Langereis MA, Zoll J, Virgen-Slane R, Peisley A, Hur S, Semler BL, van Rij RP, van Kuppeveld FJ. 2012. MDA5 detects the double-stranded RNA replicative form in picornavirus-infected cells. Cell Rep. 2:1187–1196.
26. Lindquist ME, Mainou BA, Dermody TS, Crowe JE, Jr. 2011. Activation of protein kinase R is required for induction of stress granules by respiratory syncytial virus but dispensable for viral replication. Virology 413:103–110.
27. Khaperskyy DA, Hatchette TF, McCormick C. 2012. Influenza A virus inhibits cytoplasmic stress granule formation. FASEB J. 26:1629–1639.
28. Simpson-Holley M, Kedersha N, Dower K, Rubins KH, Anderson P, Hensley LE, Connor JH. 2011. Formation of antiviral cytoplasmic granules during orthopoxvirus infection. J. Virol. 85:1581–1593.
29. Emara MM, Brinton MA. 2007. Interaction of TIA-1/TIAR with West Nile and dengue virus products in infected cells interferes with stress granule formation and processing body. Proc. Natl. Acad. Sci. U. S. A. 104:9041–9046.
30. Qin Q, Hastings C, Miller CL. 2009. Mammalian orthoreovirus particles induce and are recruited into stress granules at early times postinfection. J. Virol. 83:11090–11101.
31. Langereis MA, Feng Q, van Kuppeveld FJ. 27 March 2013. MDA5 localizes to stress granules but this localization is not required for the induction of type I interferon. J. Virol. doi:10.1128/JVI.03213-12.
32. Barral PM, Morrison JM, Drahos J, Gupta P, Sarker D, Fisher PB, Racaniello VR. 2007. MDA-5 is cleaved in poliovirus-infected cells. J. Virol. 81:3677–3684.
33. Barral PM, Sarkar D, Fisher PB, Racaniello VR. 2009. RIG-I is cleaved during picornavirus infection. Virology 391:171–176.
34. Iseni F, Garcin D, Nishio M, Kedersha N, Anderson P, Kolakofsky D. 2002. Sendai virus trailer RNA binds TIAR, a cellular protein involved in virus-induced apoptosis. EMBO J. 21:5141–5150.
35. Ricour C, Delhaye S, Hato SV, Olenyik TD, Michel B, van Kuppeveld FJ, Gustin KE, Michiels T. 2009. Inhibition of mRNA export and dimerization of interferon regulatory factor 3 by Theiler's virus leader protein. J. Gen. Virol. 90:177–186.
36. Delhaye S, van Pesch V, Michiels T. 2004. The leader protein of Theiler's virus interferes with nucleocytoplasmic trafficking of cellular proteins. J. Virol. 78:4357–4362.
37. Paul S, Michiels T. 2006. Cardiovirus leader proteins are functionally interchangeable and have evolved to adapt to virus replication fitness. J. Gen. Virol. 87:1237–1246.
38. Hato SV, Ricour C, Schulte BM, Lanke KH, de Bruijni M, Zoll J, Melchers WJ, Michiels T, van Kuppeveld FJ. 2007. The mengovirus leader protein blocks interferon-alpha/beta gene transcription and inhibits activation of interferon regulatory factor 3. Cell. Microbiol. 9:2921–2930.

Int. J. Mol. Sci. **2014**, *15*, 58-74; doi:10.3390/ijms15010058

OPEN ACCESS
International Journal of
Molecular Sciences
ISSN 1422-0067
www.mdpi.com/journal/ijms

Article

Chimeric Mice with Humanized Livers: A Unique Tool for *in Vivo* and *in Vitro* Enzyme Induction Studies

Masakazu Kakuni [1], Chihiro Yamasaki [1], Asato Tachibana [1], Yasumi Yoshizane [1], Yuji Ishida [1,2] and Chise Tateno [1,2,*]

[1] PhoenixBio Co., Ltd., 3-4-1, Kagamiyama, Higashihiroshima, Hiroshima 739-0046, Japan; E-Mails: masakazu.kakuni@phoenixbio.co.jp (M.K.); chihiro.yamasaki@phoenixbio.co.jp (C.Y.); atachibana@phoenixbio.co.jp (A.T.); yyoshizane@phoenixbio.co.jp (Y.Y.); yuji.ishida@phoenibio.co.jp (Y.I.)

[2] Liver Research Project Center, Hiroshima University, 1-2-3 Kasumi, Minami, Hiroshima, Hiroshima 734-8551, Japan

* Author to whom correspondence should be addressed; E-Mail: chise.mukaidani@phoenixbio.co.jp; Tel.: +81-82-431-0016; Fax: +81-82-431-0017.

Received: 1 November 2013; in revised form: 5 December 2013 / Accepted: 6 December 2013 / Published: 20 December 2013

Abstract: We performed *in vivo* and *in vitro* studies to determine the induction of human cytochrome P450 (CYP) using chimeric mice with humanized liver (PXB-mice®) and human hepatocytes isolated from the PXB-mice (PXB-cells), which were derived from the same donor. For the *in vivo* study, PXB-mice were injected with 3-methylcholanthrene (3-MC, 2 or 20 mg/kg) or rifampicin (0.1 or 10 mg/kg) for four days. For the *in vitro* study, PXB-cells were incubated with 3-MC (10, 50, or 250 ng/mL) or with rifampicin (5 or 25 μg/mL). The *CYP1A1* and *1A2*, and *CYP3A4* mRNA expression levels increased significantly in the PXB-mouse livers with 20 mg/kg of 3-MC (C_{max}, 12.2 ng/mL), and 10 mg/kg rifampicin (C_{max}, 6.9 μg/mL), respectively. The *CYP1A1* mRNA expression level increased significantly in PXB-cells with 250 ng/mL of 3-MC, indicating lower sensitivity than *in vivo*. The *CYP1A2* and *CYP3A4* mRNA expression levels increased significantly with 50 ng/mL of 3-MC, and 5 μg/mL of rifampicin, respectively, which indicated that the sensitivities were similar between *in vivo* and *in vitro* studies. In conclusion, PXB-mice and PXB-cells provide a robust model as an intermediate between *in vivo* and *in vitro* human metabolic enzyme induction studies.

Keywords: liver; P450 induction; humanized animal model; rifampicin; 3-methylcholanthrene

1. Introduction

Metabolic enzyme induction is a side effect of some drugs, and it can cause important problems in drug metabolism and toxicity, such as a reduction in a drug's effect and an increase in reactive metabolites. It is, thus, necessary to evaluate the induction potential of drugs in humans during preclinical drug development. However, such predictions are difficult to test because there are species differences between humans and laboratory animals in metabolic enzyme inducibility. There is also limited availability of donated human liver samples.

Previously, chimeric mice with humanized livers were generated by transplanting cryopreserved human hepatocytes into the spleen of urokinase-type plasminogen activator (uPA)/severe combined immunodeficient (SCID) mice [1,2]. In the liver of the chimeric mouse (PXB-mouse®) we developed, mouse hepatocytes are largely repopulated with the transplanted human hepatocytes, which have been demonstrated to express human cytochrome P450 (CYP) enzymes [3], phase II enzymes [4], and transporters [5], and have the potential for CYP enzyme induction with inducers [2]. Recently, other human liver chimeric mice were generated using *Fah*$^{-/-}$/*Rag2*$^{-/-}$/*Il2rg*$^{-/-}$ mice and TK-NOG mice and humanized livers from these mice expressed human CYP mRNA at similar levels as human hepatocytes [6,7]. As treatment of the mice with inducers results in *in vivo* enzyme induction in the humanized hepatocytes, the animals chimeric mice enable the evaluation of enzyme inducing effects would be useful in predicting enzyme induction in humans.

In vitro enzyme induction studies are routinely conducted during drug development at pharmaceutical companies, and very large numbers of human hepatocytes are used in such studies to predict the potential for enzyme induction. Many of the human hepatocytes used in such *in vitro* enzyme induction studies are supplied fresh, due to advantages in terms of cell function, primarily plating efficiency in dishes, as compared with cryopreserved human hepatocytes. However, it is difficult to obtain fresh human hepatocytes for *in vitro* studies, including enzyme induction studies, due to their limited availability. Additionally, preparing fresh human hepatocytes ahead of time and performing reproducible studies using the same donor cells are not possible.

In contrast, our chimeric mice possess live human hepatocytes in the liver and fresh human hepatocytes from the chimeric mouse (PXB-cells) are thus considered to be a suitable model to be used in place of fresh human hepatocytes for *in vitro* studies. The availability of cryopreserved human hepatocytes isolated from the chimeric mice has been established in evaluating the induction of hCYP1A2 and hCYP3A4 in previous studies [8,9] and a recent study demonstrated repeated and on-demand availability of fresh chimeric human hepatocytes derived from the same donor using these chimeric mice [10]. However, there have been no studies in which induction abilities of human hepatocytes were directly compared between *in vivo* and *in vitro* conditions.

In the present study, we investigated enzyme induction *in vivo* in the intact chimeric mice, and *in vitro* using fresh chimeric human hepatocytes derived from the same donor. Our result demonstrates that the unique *in vivo*/*in vitro* human hepatocyte model provides robust information to prove the